Ground-Based Technologies for Cotton Root Rot Control: Results from a Three Year Experiment

Curtis D. Cribben, J. Alex Thomasson, Yufeng Ge, Cristine L.S. Morgan
Texas A&M University, College Station, TX
Chenghai Yang, USDA ARS, College Station, TX
Robert L. Nichols, Cotton Incorporated, Cary, NC

Abstract:

The overall goal of this research is to develop ground-based technologies for disease detection and mapping which can maximize the effectiveness and efficiency of CRR (cotton root rot) treatments. Accurately mapping CRR could facilitate a much more economical solution than treating entire fields. Three cotton fields around CRR-prone areas of Texas have been the sites for three years of data collection. Freshly picked cotton leaves from healthy, disease-stressed, and dying or dead plants were scanned with an ASD VisNIR spectroradiometer. Within each plot, moisture, temperature, and bulk electrical conductivity of surface soil were measured with a Delta-T WET sensor or moisture only with a Theta Probe. A thermal infrared camera was used to capture leaf canopy images of healthy and disease-stressed plants. A complete soil ECa (apparent electrical conductivity) survey was conducted for each field with an EM-38 sensor. Plant status was visually inspected and recorded to form a series of disease-progression maps in each field. Leaf spectra have been evaluated with LDA (linear discriminant analysis) to relate them to classifications of infection level. Multiple linear regression was used to relate physical and chemical soil properties to the ECa values obtained from the EM-38. These data continue to be analyzed to (1) understand the spatiotemporal progression of CRR and (2) identify promising means for its detection.

Introduction:

Phymatotrichum omnivorum, otherwise known as cotton root rot (CRR), is a highly destructive fungus affecting dicotyledonous plants in the southwestern United States and northern Mexico (Uppalapati et al., 2010). Speculation suggests the fungus' range is limited by cooler temperatures to the north and by nonconductive soil types to the east (Percy, 1983). CRR penetrates the roots of broadleaf plants and blocks the flow of water from the roots to the leaves for transpiration, causing the leaves to wilt (Olsen et al., 1983). In general the fungus will not infect entire fields (Lyda, 1978); instead it will begin from different locations

throughout the field and spread in circular patterns from those foci (Uppalapati et al., 2010). Due to the added stress the fungus puts on the plant, infected plants usually produce a lower lint yield (Ezekiel and Taubenhaus, 1934) and lower quality cotton (Taubenhaus and Ezekiel, 1935) than healthy plants from the same field. Yield and quality are the principal determiners of profitability in cotton production, meaning that CRR can have serious effects on profitability.

The widespread effects of CRR have brought about several treatment methods with limited success. Cotton plant roots with lower carbohydrate concentrations were shown to be more susceptible to CRR, but no cost-effective method for raising the concentrations was found (Eaton and Rigler, 1946). Elevated carbon dioxide in the soil facilitates the growth of CRR while possibly suppressing the growth of competing microbes (Lyda and Burnett, 1975). This idea explains why many have used deep plowing to aerate the soil and minimize the occurrence of CRR; however, this treatment will not permanently eradicate the disease (Shear, 1908). An attempt has also been made to breed resistant cultivars, however, experiments under controlled conditions found no evidence of plant tolerance or resistance (Percy and Rush, 1985). Plant spacing has also been looked at as a means to limit the spread of CRR (Koch et al., 1987). They found that plant spacing of 20-69 cm could limit the spread of CRR within a field. More than likely the lower yields resulting from the low plant density have eliminated this as a control measure.

Several chemical compounds have also been examined for their influence on disease spread. In one instance sodium chloride was found to be effective in lowering disease incidence in soils known to be infested with the fungus (Taubenhaus et al., 1932). Furthermore, a positive correlation was found between high levels of exchangeable sodium in the soil and the absence of CRR (Lyda and Kissel, 1974). However, field tests in Arizona showed no significant difference in sodium levels between infested and non-infested areas (Mueller et al., 1983). Further field trials by Mueller et al. (1983) demonstrated that sodium chloride application did not affect CRR incidence in Arizona fields. Recently, Isakeit et al. (2010) have explored methods involving the chemical flutriafol, which has been successful in reducing the severity of CRR.

Soil apparent electrical conductivity (ECa) lends itself as a very useful tool considering some of the established relationships between CRR and different soil properties. Factors influencing ECa include soil texture, bulk density, salinity, and water content (Corwin et al., 2003). Akbar et al. (2004) found that ECa measurements from an EM-38 sensor (Geonics Limited, Mississauga, Ontario, Canada) could be useful in estimating the depth to the soil carbonate layer in Texas Vertisols. The ability of ECa instruments to quickly and accurately map soil properties is of great value; however it is difficult to apply relationships found in one study to additional studies concerning different soil types. No work has been done at the field scale to compare soil properties to ECa and the presence of CRR. ECa measurements using the EM-38 are an inexpensive way of rapidly obtaining large amounts of spatially referenced data which can be linked to soil characteristics.

Jeger et al. (1987) attempted to quantify the spread of CRR temporally as well as spatially throughout the growing season. They observed two notable trends from their nearest neighbor analysis. The first trend was that disease spread within the row was more important during the early stages of the disease. Second, the appearance of new and isolated disease incidences within the plot was not constant throughout the season. Their study suggests that spatiotemporal statistical models should be explored further as a means to describe plant disease epidemics more effectively.

Early detection methods for diagnosing plants infected with CRR used infrared thermometry (Pinter et al., 1979). Using a hand-held infrared thermometer they were able to accurately diagnose plants in Arizona cotton fields. In an effort to increase the economic feasibility of treatment methods and diagnose large cotton fields quickly, Yang et al. (2005) used the following process to identify problem areas using remote sensing. Multispectral aerial images of a cotton field's canopy in three spectral bands (near infrared, red, and green) were classified into areas of healthy or diseased plants, assuming that the main stress present was CRR. The resulting disease maps were modified to include the minute healthy areas within largely infected areas as they were too small for farm equipment to practically avoid. A buffer zone was then added around the infected areas to account for disease spread. The final maps served to display treatment areas of the cotton field for precision application. Previous research has not as yet produced a user-friendly, cost-effective, ground-based solution for the identification and precision treatment of CCR. The objectives of this project are to first understand the spatiotemporal progression of CRR in a production cotton field, and second to develop a ground-based method for mapping plant infection. This paper will focus on the most recently completed research concerning both objectives.

Materials and Methods:

Three different areas in Texas with an established history of cotton root rot were observed during the 2010-2012 growing seasons for this study. The first plot was used throughout all three years and was located in a rainfed field on the Stiles Farm and Texas A&M Research Center at Thrall, in the Northern Blackland Prairies of Texas. The second plot was also used all three years and was located in a drip irrigated field in the Red Prairies of Texas near San Angelo. The third plot was located in the Southern Subhumid Gulf Coastal Prairies of Texas. In years one and two a drip irrigated plot outside of Sinton was used whereas in year three the plot was located in a rainfed field closer to Corpus Christi. Each plot measured 24 rows wide by approximately 45 yards (45 paces) long, and data collection for the each location was roughly based on a weekly schedule. A detailed description of the data collected during each plot visit is discussed in Cribben et al. (2011).

Disease maps were created of the plot during each visit made. The health of plants was rated on a scale from one to four going from healthy to dead. A number was assigned for the plants in each of the 45 paces in all 24 rows resulting in a grid of 1,080 observations.

Disease maps were plotted using ArcGIS (ESRI, Redlands, CA) to give a visual representation of the disease progression (figure 1). The percentage of infected plants within the plot was also graphed against the Julian date to display the temporal spread of the disease (figures 2 and 3). Spatial aggregation analysis will be completed to determine if a spatial relationship exists for the spreading of CRR

On each visit reference leaf samples were collected to provide examples of each disease stage one through four. Leaves were collected at the plot and stored in plastic zipper bags which were placed inside a cooler on ice. Once all samples were collected, the cooler was taken back to the lab where the leaves were analyzed. The leaf collection procedure was based on a study done by Thomasson and Sui (2009) that proved this method to have minimal effects on leaf reflectance spectra within 6 hours of picking. Each leaf was then scanned twice with the ASD VisNIR spectroradiometer (ASD Inc., Boulder, CO) to give the reflectance spectrum that could be used to classify the leaves. Linear discriminant analysis (LDA) was used to examine the reference leaves and determine which bands in the spectra were most useful in classifying the leaves as healthy or infected. Future work using wavelet analysis may prove even more useful to the classifying process.

An ECa survey was performed at the Thrall, San Angelo, and Sinton locations between the 2010 and 2011 growing seasons using an EM-38 sensor. The EM-38 was pulled inside a wooden sled behind an all-terrain vehicle. The vertical and horizontal dipoles on the EM-38 measure soil ECa to depths of 1.5 m and 0.75 m respectively (McNeill, 1992). A Trimble GPS unit (Trimble Navigation Limited, Sunnyvale, CA) was used spatially reference the ECa data. As the EM-38 was pulled through the field, the ECa measurements and the GPS coordinates were recorded every second. Passes were made approximately every 4.5 m to maximize map resolution without collecting redundant data. The ECa data was split into three equal sized categories representing the high, medium, and low thirds of ECa measurements taken at each location. This data was imported into ArcGIS as a means to map the soil ECa in relation to features in the field's aerial images.

Soil cores were taken at the surveyed locations to obtain samples representative of the ECa measurements and CRR incidence. CRR infected areas were defined based on visual assessment of the aerial images. Six categories were established based on the healthy and infected areas of the aerial images and the high, medium, and low ECa areas seen in each survey. Soil cores were collected from each of the six categories using a soil coring truck equipped with a Giddings Probe (Giddings Machine Company, Windsor, CO). At the Thrall location six cores were taken to a depth of approximately 1.6 m unless obstructions prohibited the probe from going deeper. The 23 soil cores collected from the Sinton location were taken down to the soil parent material giving an average core depth of 1.4 m. The 22 San Angelo location soil cores were also taken to the depth of parent material when conditions allowed resulting in an average core depth of 1.1 m when the probe was unimpeded. All cores were collected in plastic sleeves which were capped and transported to the Texas A&M University hydropedology laboratory for analysis. Each soil core was cut

apart and described by horizon with a sample from each horizon being ground up and passed through a two millimeter sieve. The depth at which soil matrix effervescence first occurred was recorded along with the depth where the first calcium carbonate nodules appeared. A pH meter and EC meter were used to find the pH and test EC for each soil core horizon. Each horizon's texture was found through soil particle size analysis using the pipette method as described by Kilmer and Alexander (1949). Also, cation abundance was found by measuring the inorganic carbon content of each horizon sample through the pressure-calcimeter method as described by Sherrod et al. (2002). Multiple linear regression was used to relate the different soil properties to the ECa measurement taken in the field. T-tests were used to look for any significant soil property differences between cores pulled from infected areas of the field and those taken from healthy ones.

Results:

The disease maps from the San Angelo plot give an example of the data that have been collected over the 2010, 2011, and 2012 growing seasons. The grid cells in the plot have been colored to better represent the disease severity. Figure 1 is based on the scale described earlier where healthy plants are represented by the number one and increasing disease severity uses numbers two through four. In figure 1 the color green to corresponds to the numerical value of one and as the scale goes from two to three to four the colors change from pale green to orange to red.

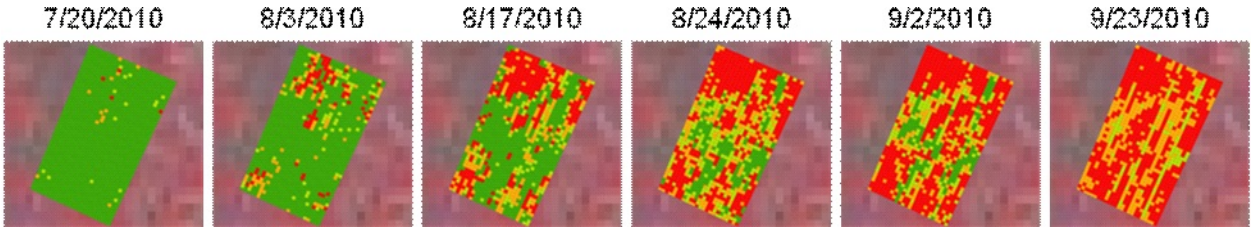

Figure 1. The disease map from each visit to the San Angelo plot in 2010 (1: healthy = green, 2: disease stage 1 = yellow-green, 3: disease stage 2 = orange, 4: dead = red)

The disease maps visually demonstrate how the disease varies in time and space throughout the growing season. To isolate the temporal variation of CRR during each growing season the percentage of infected plants was graphed according to the Julian date when it was observed. Figures 2 and 3 give the disease progression graphs for Thrall and San Angelo respectively.

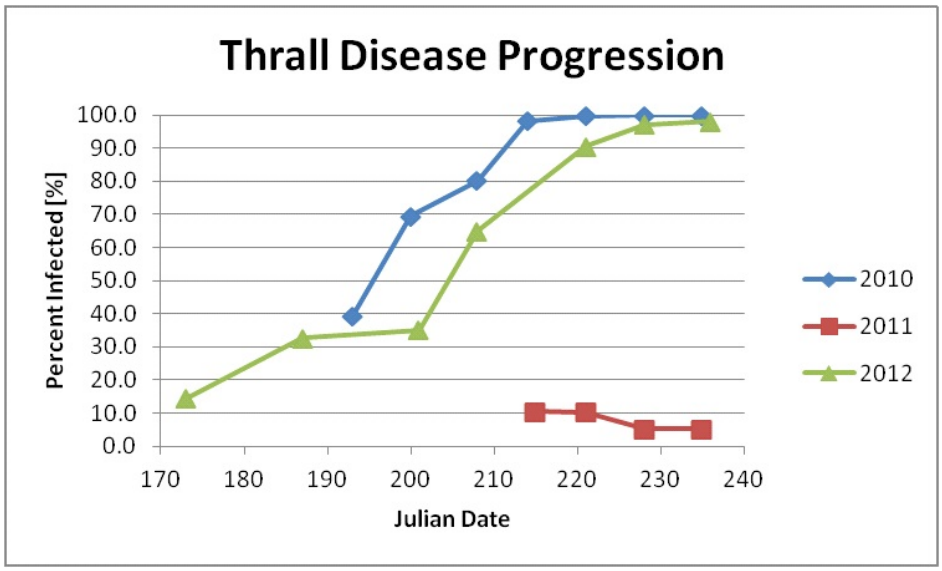

Figure 2. The Thrall disease progression graph for .all three growing seasons

Disregarding the severe drought of 2011, Thrall shows an extremely similar rate of infection within the plot. This trend suggests that there is similar temporal behavior of CRR from one year to the next assuming environmental conditions are consistent.

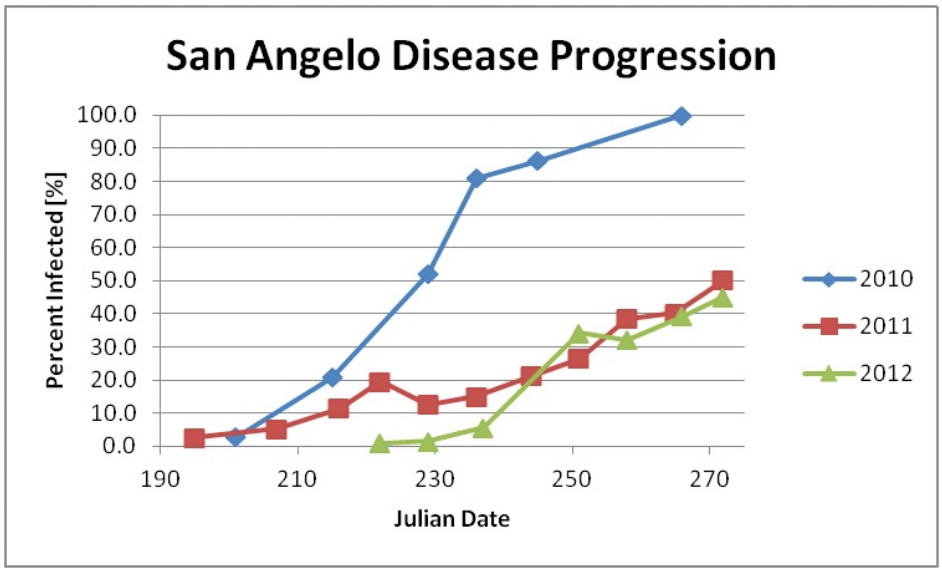

Figure 3. The San Angelo disease progression graph for all three growing seasons

The plants in the San Angelo plot were more water stressed in 2011 and 2012 than in 2010. The similar weather conditions appear to have affected the spread of CRR in approximately the same manner. The lack of water is not expressed the same way in San Angelo as in Thrall because of the drip irrigation system in place at San Angelo. Both figure 2 and figure 3 imply that under similar conditions the spread of CRR is consistent in its

temporal variation. Data analysis examining the aggregation of CRR incidence within the field plot will help to fully understand the spatiotemporal progression of CRR.

The LDA of the reference leaf spectra identified wavelength bands which are useful in classifying healthy or infected leaves. Table 1 gives the results of the best model using the 2010 and 2011 reference leaf data.

Table 1. The results of the linear discriminant analysis (LDA) showing a potential 90% classification rate

		predicted	
		H	I
actual	H	35	15
	I	5	147

To get these results, leaves of category two, three, and four were combined to form one category of infected samples represented by "I" in table 1. Samples originally in category one were relabeled as healthy and are represented by "H" in table 1. The actual data, in the rows of table 1, show that there were 50 healthy samples and 152 infected samples observed in this data set. The actual sample categories were compared to the computer model predicted categories. The computer model incorrectly classified 15 of the healthy leaf spectra as infected and 5 of the infected spectra as healthy. Overall, the computer model placed 90% of the leaf spectra into the right categories. This specific model used 50nm wide bands centered at 525, 2075, 2175, and 2325 nm. In order to design the most accurate and cost-effective sensor the data from the 2012 growing season must be added to the model, wavelet analysis must be done to the full data set, and a cost analysis of the required optical components must be completed.

Figure 4 shows the San Angelo ECa map and the soil core locations overlaid on top of the aerial image. Coring points were chosen to sample the full range of ECa values as well as areas with and without signs of CRR. An attempt was made to directly correlate the ECa measurement with the presence of CRR. A weak relationship existed at the San Angelo location, but was not duplicated in either of the other fields.

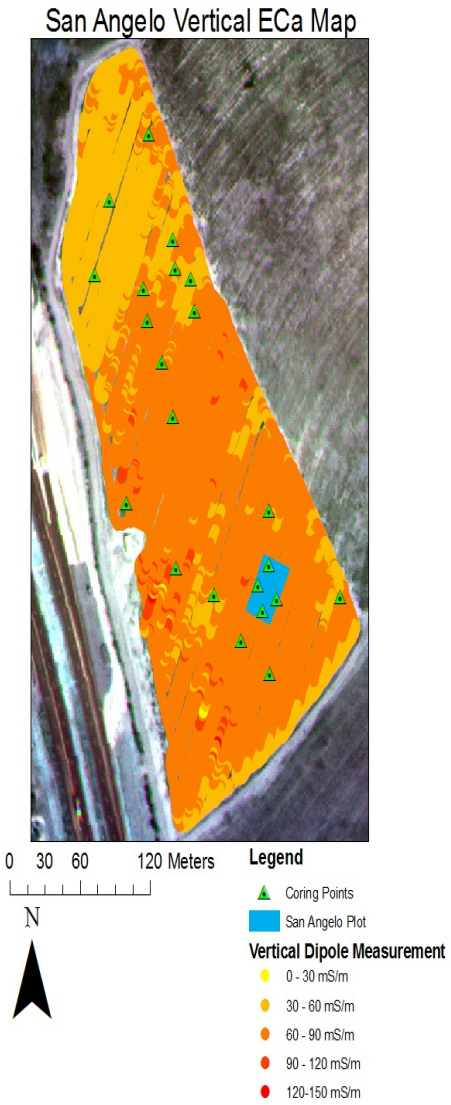

Figure 4. The ECa map of the San Angelo field with markings for the coring points (green triangles) and the test plot (blue rectangle)

Multiple linear regression was used to determine which soil properties ECa was related to since the CRR relationship did not exist. The models that best accounted the variation in ECa measurements are shown in table 2. Thrall showed a strong relationship between ECa and soil matrix effervescence as well as clay content from 50 to 60 cm. Models with more terms were not considered for Thrall because only six cores were taken at that location as compared to over 20 at each other location. Additional terms in the Thrall model were clearly over fitting the data, and not indicating the true relationship to soil ECa. The strongest relationship seen in the Sinton data was to clay with soil matrix effervescence adding a second significant term to the model. A three term model was not considered for Sinton because any additional term was not significant at the $\alpha=0.05$ level. The San Angelo

data produced models of one, two, and three significant terms that could describe a large portion of the variability seen in the soil ECa measurements.

Table 2. The models created based on each location's data, the terms used in those models, and how well the models accounted for variation in the soil ECa measurements

Location	Terms in model	Term 1	Term 2	Term 3	Model R^2
Thrall	1	Matrix Eff.[a]			0.86
	1	Clay[b] 50-60 cm			0.72
Sinton	1	Clay[b] 50-70 cm			0.16
	2	Clay[b] 50-60 cm	Matrix Eff.[a]		0.34
San Angelo	1	Clay[b] 20-40 cm			0.50
	2	Clay[b] 15-45 cm	Sand[c] 50-60 cm		0.75
	3	Clay[b] 60-90 cm	Sand[c] 30-40 cm	IC[d] 70-80 cm	0.82

[a] Matrix Eff. = The depth at which the soil matrix effervesced when in contact with HCl

[b]Clay = The percent clay content of the soil at the specified depth

[c]Sand = The percent sand content of the soil at the specified depth

[d]IC = The inorganic carbon content of the soil in grams per kilogram at the specified depth

These results relate well to what the literature leads us to expect. Higher soil clay contents are known to have a larger water holding capacity, and soil moisture as well as clay content are factors which influence soil ECa (Corwin et al., 2003). Using that same logic, a negative correlation to the sand content could exist due to the poor water holding capabilities of sand. The results also suggest that calcium carbonate levels are mapped by the EM-38 through the soil properties of inorganic carbon content and soil matrix effervescence. It is unknown how clay, sand, and calcium carbonate influence the propagation of CRR throughout the field, but a further understanding of those relationships could lead to better treatment methods for the disease.

T-tests were run on all soil properties to determine if a significant difference existed between the soil cores pulled from healthy areas of the field and those pulled from infected areas. Preliminary results showed statistically significant differences in San Angelo and Sinton where the datasets were larger, but not in Thrall. There was not an overwhelming trend in the significant soil traits found at either location. However, the vast majority of significant soil traits were in the top 30 cm of soil. Further work will be done to determine if these preliminary results can be justified.

Conclusions:

Three important conclusions can be drawn from the recently completed research:

The temporal spread of CRR in production cotton fields appears consistent given similar weather conditions.

An optoelectronic sensor can be designed to accurately classify cotton plants infected with CRR.

Soil ECa cannot directly map CRR, but instead tends to map soil properties related to the hydrological characteristics of the soil.

Acknowledgments:

The authors of this paper would like to thank Cotton Incorporated and the Texas state Support Committee for providing funding for this project. Also, special thanks go out to Mr. Miles Moudy, Ms. Sonia Zamarripa, all of Dr. Cristine Morgan's students, and the producers and extension agents for helping with data collection.

References:

Akbar, M.A., A.L. Kenimer, and S.W. Searcy. 2004. Estimating soil profile depth with apparent electrical conductivity for a Texas Vertisol. *Trans. ASABE* 47(4): 1087-1092.

Corwin, D.L., S.R. Kaffka, J.W. Hopmans, Y. Mori, J.W. van Groenigen, C. van Kessel, S.M. Lesch, and J.D. Oster. 2003. Assessment and field-scale mapping of soil quality properties of a saline-sodic soil. *Geoderma* 114: 231-259.

Cribben, C.D., J.A. Thomasson, Y. Ge, M.D. Korte, C.L.S. Morgan, C. Yang, R.L. Nichols. 2011. Ground-based technologies for cotton root rot control. *Beltwide Cotton Conf. Proc*., 552-558. Cordova, TN: National Cotton Council.

Eaton, F.M., and N.E. Rigler. 1946. Influence of carbohydrate levels and root-surface microfloras on phymatotrichum root rot in cotton and maize plants. *J. Agric. Res.* 72(4): 137-161.

Ezekiel, W.N., and J.J. Taubenhaus. 1934. Cotton crop losses from phymatotrichum root rot. *J. Agric. Res.* 49(9): 843-858.

Isakeit, T., R. Minzenmayer, A. Abrameit, G. Moore, and J.D. Scasta. 2010. Control of phymatotrichopsis root rot of cotton with flutriafol. *Beltwide Cotton Conf. Proc.*, 200-203. Cordova, TN: National Cotton Council.

Jeger, M.J., C.M. Kenerley, T.J. Gerik, and D.O. Koch. 1987. Spatial dynamics of phymatotrichum root rot in row crops in the blackland region of north central Texas. *Phytopathol*. 77(12): 1647-1656.

Kilmer, V.H., L.Z. Alexander. 1949. Methods for making mechanical analyses of soils. *Soil Sci.* 68: 15-24.

Koch, D.O., M.J. Jeger, T.J. Gerik, and C.M. Kenerley. 1987. Effects of plant density on progress of phymatotrichum root rot in cotton. *Phytopathol*. 77(12): 1657-1662.

Lyda, S.D. 1978. Ecology of phymatotrichum omnivorum. *Ann. Rev. of Phytopathol*. 16: 193-209.

Lyda, S.D., and E. Burnett. 1975. The role of carbon dioxide in growth and survival of Phymatotrichum omnivorum. In *Biol. Control Soil-borne Plant Pathogens Intl.Symp.,* 63-68 G. W. Bruehl, ed. St. Paul, MN: Am. Phytopathol. Soc.

Lyda, S.D., and D.E. Kissel. 1974. Sodium influence on disease development and sclerotial formation by phymatotrichum omnivorum. *Proc. of the American Phytopathol. Soc.,* 163-164. St. Paul, MN: APS Press.

McNeill, J.D. 1992. Rapid, accurate mapping of soil salinity by electromagnetic ground conductivity meters. In *Advances in Measurement of Soil physical Properties: Bringing Theory into Practice*, 209-229. G.C. Topp, W.D. Reynolds, R.E. Green, eds. Special Publication No. 30. Madison, WI: SSSA.

Mueller, J.P., R.B. Hine, D.A. Pennington, and S.J. Ingle. 1983. Relationship of soil cations to the distribution of phymatotrichum omnivorum. *Phytopathol*. 73(10): 1365-1368.

Olsen, M.W., I.J. Misaghi, D. Goldstein, and R.B. Hine. 1983. Water relations in cotton plants infected with phymatotrichum. *Phytopathol*. 73(2): 213-216.

Percy, R.G. 1983. Potential range of phymatotrichum omnivorum as determined by edaphic factors. *Plant Disease* 67(9): 981-983.

Percy, R.G., and C.M. Rush. 1985. Evaluation of four upland cotton genotypes for a rate-limiting resistance of phymatotrichum root rot. *Phytopathol*. 75(4): 463-466.

Pinter, P.J. Jr., M.E. Stanghellini, R.J. Reginato, S.B. Idso, A.D. Jenkins, and R.D. Jackson. 1979. Remote detection of biological stresses in plants with infrared thermometry. *Science* 205(4406): 585-587.

Shear, C.L. 1908. Texas root-rot of cotton; field experiments in 1907. *USDA Bur. Plant Ind.* Cir. 9 1-7.

Sherrod, L.A., G. Dunn, G.A. Peterson, R.L. Kolberg. 2002. Inorganic carbon analysis by modified pressure-calcimeter method. *Soil Sci. America J.* 66: 299-305.

Taubenhaus, J.J. and W.N. Ezekiel. 1935. The quality of lint and seed from cotton plants with phymatotrichum Root Rot. *Phytopathol*. 25: 104-113.

Taubenhaus, J.J. W.N. Ezekiel, and J.F. Fudge. 1932. Incidence of root rot as affected by field additions of fertilizer and other salts to the soil. *Texas Agric. Exp. Station Ann. Reports* 45: 70.

Thomasson, J.A., R. Sui. 2009. Cotton leaf reflectance changes after removal from the plant. *J. Cotton Sci.* 13: 206-211.

Uppalapati, S.R., C.A. Young, S.M. Marek, and K.S. Mysore. 2010. Phymatotrichum (cotton) root rot caused by phymatotrichopsis omnivora: retrospects and prospects. *Molecular Plant Pathol.* 11(3): 325-334.

Yang, C., C.J. Fernandez, and J.H. Everitt. 2005. Mapping phymatotrichum root rot of cotton using airborne three-band digital imagery. *Trans. ASABE* 48(4): 1619-1626.